Flexible Control for Wide Speed Range Operation of High Polarity Stator Coreless AFPM Machines with WBG Semiconductor Devices

Yaser Chulaee[1], Ali Mohammadi[1], Aaron Cramer[2], Dan M. Ionel[1]
[1]SPARK Laboratory, Stanley and Karen Pigman College of Engineering, University of Kentucky, Lexington, KY, USA
[2]ECE Department, Stanley and Karen Pigman College of Engineering, University of Kentucky, Lexington, KY, USA

yaser.chulaee@uky.edu, alimohammadi@uky.edu, aaron.cramer@uky.edu, dan.ionel@ieee.org

***Abstract*—This paper presents a dual-mode controller designed to enable a high-polarity coreless stator axial flux PM (AFPM) machine to operate over a wide range of speeds. The proposed approach includes a combination of sine-wave (field-oriented) and square-wave control schemes. Coreless machines offer the advantage of being effortlessly controlled using square-wave voltages, thanks to the absence of core losses and negligible torque ripple caused by the lack of a magnetic core. By adopting square-wave control, the need for high-precision encoders is eliminated, enabling the utilization of Hall effect sensors or sensorless drive schemes instead. This, in turn, facilitates the attainment of ultra-high speeds with enhanced efficiency. The square-wave control mode also extends the machine speed range while fully utilizing the DC-link voltage. The control system is implemented on full-bridge inverters based on wide bandgap (WBG) semiconductor devices operating at high switching frequencies. This is done to minimize current ripple due to the ultra-low inductance of this type of machines. The machine performance was simulated using finite element analysis (FEA) and MATLAB/Simulink, and it was also experimentally tested on a prototype two-phase PCB stator coreless AFPM machine connected to two single-phase full-bridge inverters.**

***Index Terms*—Axial-flux, coreless machines, FEA, permanent-magnet machines, PCB stator, drive-systems, field oriented control, square-wave control, sensorless control, wide bandgap semiconductors.**

I. Introduction

Coreless axial flux permanent magnet (AFPM) machines offer unique advantages over conventional cored electric machines. Due to the lack of a magnetic core and the associated power losses, there is potential for an increase in machine efficiency and torque density [1]. Furthermore, in the absence of stator teeth, these machines do not experience cogging torque, resulting in a very smooth output torque profile and low acoustic noise [2, 3]. Additionally, the possibility to have a higher pole count leads to potential performance improvements [4]. These features make coreless machines well-suited for various high speed applications, including aerospace, precision manufacturing, electric vehicles, and industrial motor-drives [2].

Recently, there has been growing interest in integrating printed circuit board (PCB) stators into coreless AFPM machines due to their reduced weight and volume, flexible coil shape design, and potentially reliable and repeatable fabrication process [5–8]. Axial flux PM machines incorporating coreless PCB stators exhibit ultra-low phase inductance owing to a considerably wider effective airgap, providing the unique advantage of an excellent dynamic response but also presenting some control challenges [9]. The low phase inductance in coreless AFPM machines primarily results in high current ripple, which causes power losses in the rotor back-iron, magnets, and stator windings, as well as torque pulsations [10]. Additionally, it limits the flux-weakening capability to a very low level, which means the output power decreases faster above the rated speed compared to cored machines, resulting in a narrower speed range [11]. Hence, to fully leverage the distinctive features of coreless machines, the entire drive system must be appropriately designed and utilized to prevent machine performance degradation.

In order to expand the speed range of operation for such electric machines, it is necessary to implement specific measures to fully utilize the converter DC-link. Additionally, if possible, certain modifications should be made to the machine design. An integrated stator embedded inductor was proposed in [12] to improve the field weakening operation of low inductance slotless PMSM. This approach also mitigated the pulse width modulation (PWM) induced current ripple and current ripple induced core losses.

To overcome the lack of an inverter voltage source above the base speed in conventional drive systems for high-speed applications, z-source inverters with voltage boost capability were introduced in [13]. Z-source converters are able to provide flexible voltage gain and also improve the system reliability. Applying square-wave voltage to machine terminals or over-modulation at high speeds is another technique to fully utilize the inverter DC-link and push the speed limit. A new current regulator that can provide a wider operating range for PMSM operating under square-wave mode at high speed, used in rail traction systems, was proposed in [14].

To maintain the current ripple within acceptable levels, low inductance motor drives typically necessitate a switching frequency in the range of 50–100 kHz [9]. In conventional drive systems for low inductance machines, current ripple and

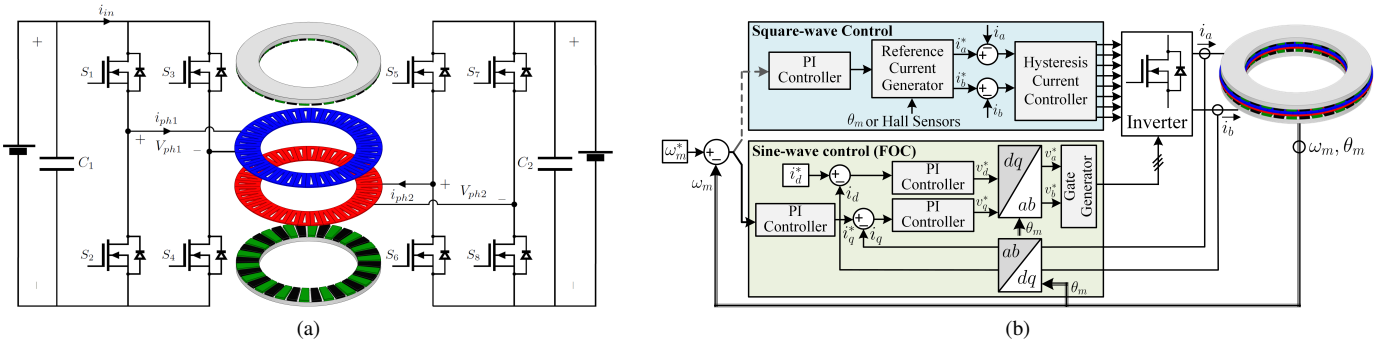

(a) (b)

Fig. 1. Independent single-phase inverters connected to PCB stators (a). The output voltages of these inverters are shifted by 90 electrical degrees with respect to each other. The block diagram of the dual-mode drive system (b). Sine-wave and square-wave control modes are used interchangeably.

PWM reflected current harmonics are reduced by using LC and LCL filters. A drawback in LC filters is that they can cause distortion in voltage and current waveforms, particularly in the LC resonant range, and can result in circulating currents between the inverter and the filter. Additionally, LCL filters can lead to increased system cost, weight, and volume [10].

Modern motor-drive systems are based on wide bandgap (WBG) semiconductor devices, leading to more efficient and lightweight converters. Wide bandgap semiconductor components possess reduced switching losses, which facilitates the design of inverters operating at very high switching frequencies [9]. These power converters are suitable for motors with low inductance and high power, requiring high switching frequencies and current regulation with a wide bandwidth to achieve acceptable current ripple, while also maintaining system efficiency and compactness.

This paper introduces a control system that incorporates two distinct operation modes, namely sine-wave and square-wave, designed for ultra-low inductance and high-polarity coreless AFPM machines. The square-wave control mode effectively extends the speed operation range by eliminating the reliance on precise position sensors at high speeds, providing a great opportunity to employ sensorless control schemes or Hall effect sensors. Additionally, the square-wave control fully utilizes the inverter DC-link voltage, leading to a further improvement in the achievable speed range. To reduce current ripple due to low phase inductance, the introduced control approach is implemented based on an inverter with a high switching frequency employing WBG semiconductor devices. The performance of the system is evaluated through finite element analysis (FEA) [15], simulations in MATLAB/Simulink, and experimentation using a prototype motor-drive test setup.

II. Machine and Drive System: Topology and Operation

In this study, the target machine is a 26-pole integral horsepower, two-phase, double-rotor, PCB stator, coreless AFPM machine. This machine is composed of two PCB stators, one for each phase, with 26 spiral-shaped coils sandwiched between two rotors previously introduced by the authors in introduced in [16, 17]. This configuration is commonly used due to its high torque and power densities and robustness [18]. The spiral coil winding topology is also popular because it can maximize torque per coil area and achieve a high number of turns [16]. In this configuration, a two-phase machine is created by shifting one PCB stator by 90 electrical degrees with respect to the other and then stacking them together.

To fully utilize the modularity of the PCB stators and improve the fault tolerance of the system, each PCB stator corresponding to one phase is connected to an independent single-phase inverter. The machine's configuration and connections to the power converters are shown in Fig. 1a. Each inverter consists of four SiC MOSFETs, recognized as wide bandgap devices that can provide fast switching with lower pwoer loss compared to conventional Si devices. The specifications and geometrical dimensions of this machine are also presented in Table I.

III. The Introduced Flexible Control Approach

To address the control challenges mentioned earlier and extend the machine speed range, this paper introduces a dual-mode drive system. The controller system has two modes: field-oriented control (FOC) and square-wave control, and can switch between them depending on the machine's operational zone. To overcome the inherent challenges related to ultra-low inductance coreless machines, the system employs a SiC-based inverter with a high switching frequency to implement the aforementioned control schemes. The following sections will investigate both operation modes and the potential advantages of the proposed control approach in improving the system's reliability and fault tolerance.

A. Field-Oriented Control (FOC)

Field-oriented control is a widely recognized technique for controlling the output torque and speed of electric machines by managing the phase currents in a rotational, i.e., direct and quadrature, reference frame. In this approach, the stator currents are transformed into flux-producing and torque-producing components, which are DC waveforms and can be independently regulated by conventional controllers to achieve predetermined objectives.

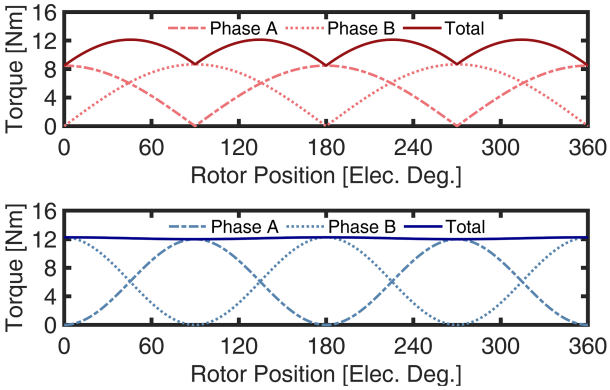

Fig. 2. The output torque waveforms of the machine under study excited by square-wave and sine-wave currents derived from 3D FEA.

In the surface mounted AFPM machine under study, the rotor is non-salient, and the derived direct (d) and quadrature (q) stator winding voltages are as follows:

$$\begin{cases} v_{sd} = R_s i_{sd} + \frac{\mathrm{d}}{\mathrm{d}t}\lambda_{sd} - \omega_s \lambda_{sq} \\ v_{sq} = R_s i_{sq} + \frac{\mathrm{d}}{\mathrm{d}t}\lambda_{sq} + \omega_s \lambda_{sd} \end{cases}; \tag{1}$$

where,

$$\begin{cases} \lambda_{sd} = L_s i_{sd} + \lambda_{pm} \\ \lambda_{sq} = L_s i_{sq} \end{cases}, \tag{2}$$

and λ_{pm} is the PM flux linkage. In these equations, R_s is the stator winding resistance, and L_s represents the stator winding inductance, which consists of the stator winding leakage inductance, L_l, and mutual inductance, L_m. The syncronous spees is also denoted by ω_s

Based on the interaction between the current in the stator windings and magnetic flux produced by rotor PMs, the two-phase output torque in the dq reference frame can be written as:

$$\begin{aligned} T_{em} &= \frac{p}{2}\left[\pi \frac{\mu_0}{l_g} r l \left(\frac{N_s}{p}\right)^2\right] \times \\ &\left[\left(i_{sq} + \frac{L_r}{L_m} i_{rq}\right) i_{rd} - \left(i_{sd} + \frac{L_r}{L_m} i_{rd}\right) i_{rq}\right] \\ &= \frac{p}{2}\left(\lambda_{sd} i_{sq} - \lambda_{sq} i_{sd}\right), \end{aligned} \tag{3}$$

where N_s is the number of turns per phase and p equals the number of poles [19]. By substituting the PM flux linkage of a non-salient pole two-phase PM machine into this equation, the output torque can be calculated as follows:

$$T_{em} = \frac{p}{2}\lambda_{pm} i_{sq} \ . \tag{4}$$

The maximum torque per ampere (MTPA) control strategy for a non-salient pole PM machine when operating below the rated speed can be achieved by setting the d-axis current i_{sd} to zero. A cascade control structure is often employed to regulate the torque-producing component of the stator current i_{sq} and achieve the desired commands. In cascade control, the inner current loop should have a higher bandwidth than the outer loops. The high switching frequency achieved by WBG semiconductor devices considerably improves the controller's bandwidth, leading to stable machine performance.

TABLE I
SPECIFICATIONS AND MAIN DIMENSIONS OF THE TARGET CORELESS PCB STATOR AFPM MACHINE.

Parameter	Value	Unit
Rated power	2.2	kW
Rated speed	1,500	rpm
Airgap (magnet to magnet)	1.3	mm
Rotor outer diameter	270	mm
Rotor inner diameter	118	mm
No. of rotor poles	26	-
No. of stator coils	26	-
Phase resistance	0.85	Ω
Phase inductance	52	μH

The block diagram depicting the FOC system for the two-phase AFPM machine is illustrated in Fig. 1b. Proportional-integral (PI) controllers are typically used in such machine control systems to generate reference voltages v_a^* and v_b^*, which are then utilized to produce gate signals for the switches. The unipolar PWM technique is employed in this control scheme featuring better efficiency and lower total harmonic distortion (THD) compared to bipolar PWM method.

The induced voltage for speeds higher than the rated speed needs to be maintained at the rated voltage. Therefore, a negative d-axis current, proportional to the increase in speed, is applied to the stator winding, which weakens the rotor magnetic field and, hence, maintains a constant induced voltage. Since in coreless machines, the phase inductance and armature reaction are not high enough, even at highly negative commands for i_{sd}, achieving effective flux weakening over a wide range of speeds is not feasible. Therefore, a square-wave control scheme, which is investigated in the following section, can extend the speed range of the machine with full utilization of the converter DC-link voltage.

B. Square-Wave Control

Square-wave control, also known as trapezoidal control, is a technique often used to operate brushless direct current (BLDC) machines with a trapezoidal-shaped back-EMF [20]. The square-wave control can also be implemented in certain applications or operational regions for PMSM machines with sinusoidal back-EMF, especially at high speeds [14]. This control method offers a straightforward implementation, eliminating the need for high-resolution encoders and complex controllers. Within this technique, phase commutations occur at specific rotor positions, which are typically determined by Hall effect sensors positioned on the stator. This control method also provides an opportunity to employ sensorless control methods, leading to further simplification in the hardware system [21, 22]. Coreless AFPM machines, characterized by negligible torque ripple and no core losses, are excellent

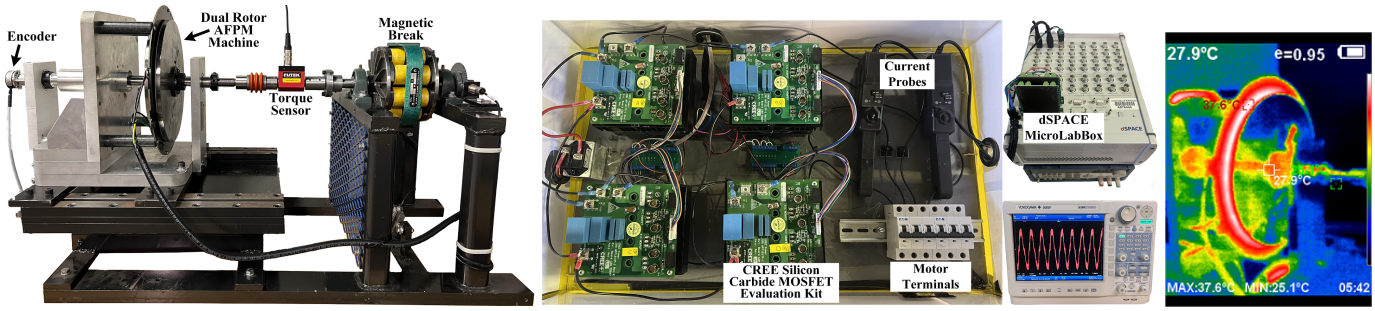

(a) (b) (c)

Fig. 3. The test bench for the target coreless AFPM machine. The machine is coupled with a magnetic break as a variable load (a). The inverter consists of four CREE 1200V SiC MOSFET modules, and the dSPACE MicroLabBox is used for HIL simulations (b). A thermal image of the machine while it is operating in FOC mode shows a negligible temperature rise in the rotor magnets and the rotor back-iron (c).

candidates for sensorless control using square-wave voltages, enabling the achievement of ultra-high speeds.

Full utilization of the DC-link is an effective technique for operation beyond the rated speed in ultra-low inductance coreless machines. In FOC mode, the peak of the fundamental component of the single-phase inverter output phase voltage is expressed as $V_{ph} = m_a V_{dc}$, where the amplitude modulation index of the sinusoidal PWM (SPWM) is $m_a \leq 1$. In order to improve the output voltage, over-modulation of SPWM may be taken into account. However, this approach can result in instability in the FOC mode and introduce additional complexity from a control perspective. In such scenarios, square-wave control can be employed to fully utilize the DC-link voltage and facilitate the control process. In this case, the peak value of the phase voltage fundamental component is $V_{ph} = 4/\pi V_{dc}$, and this improvement will be reflected in the maximum achievable speed. The block diagram of the square-wave control scheme is demonstrated in Fig. 1b. In this approach, the output currents are limited by a hysteresis controller to satisfy the commanded torque and speed [20].

The main challenge of energizing such an AFPM machine with square-wave currents is the torque ripple due to the interaction between the square-wave phase current and the sinusoidal back-EMF. The rated output torque waveforms for the machine under investigation are obtained through 3D FEA with both square-wave and sine-wave input phase currents, as illustrated in Fig. 2. Results show that the output torque is almost ripple-free when a sine-wave current is used. When square-wave currents are applied, the resulting torque waveform is composed of segments of a sine-wave which potentially leads to noise and vibration.

Since the square-wave control mode is only used at high speeds, a substantial filtering effect of the rotor moment of inertia is present. This effect effectively attenuates the adverse effects of torque ripple. The rotor of AFPM machines possesses high inertia owing to its large diameter and relatively short stack length. For instance, in the case of the machine under examination, this value stands at 4.22kg $\cdot$ m^2, which is significantly higher than that of its radial flux counterparts. It is important to acknowledge that a higher number of poles in coreless AFPM machines leads to an increased frequency in torque ripple, thereby facilitating more effective mechanical filtering.

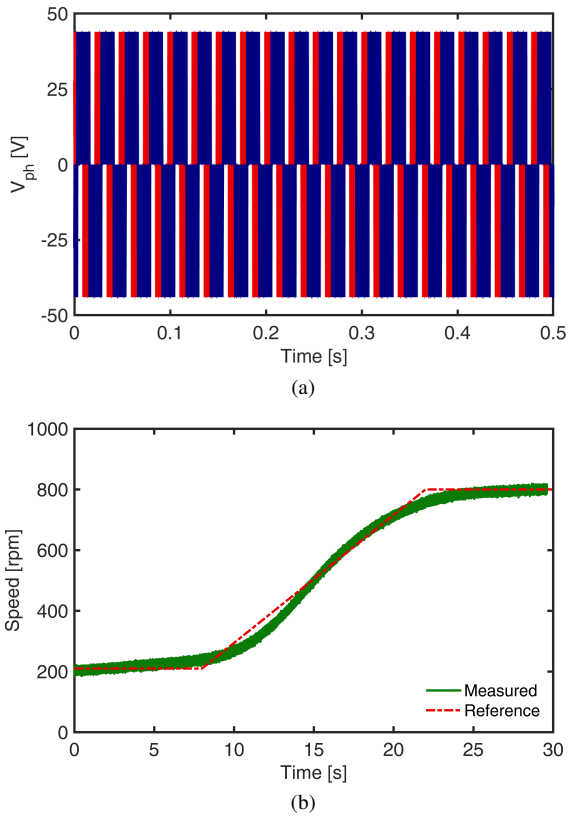

(a)

(b)

Fig. 4. The experimental performance analysis results of the target coreless AFPM machine operated by field-oriented control. The inverter phase voltages and rotor speed with a change in speed command are displayed.

IV. Experimental Results and Discussions

The performance of the machine operating in both modes was evaluated through experimental testing on the test bench depicted in Fig. 3a. The prototype machine is a 26-pole, two-phase, double-rotor, PCB stator, coreless AFPM machine which is coupled with a magnetic brake as a variable load. The

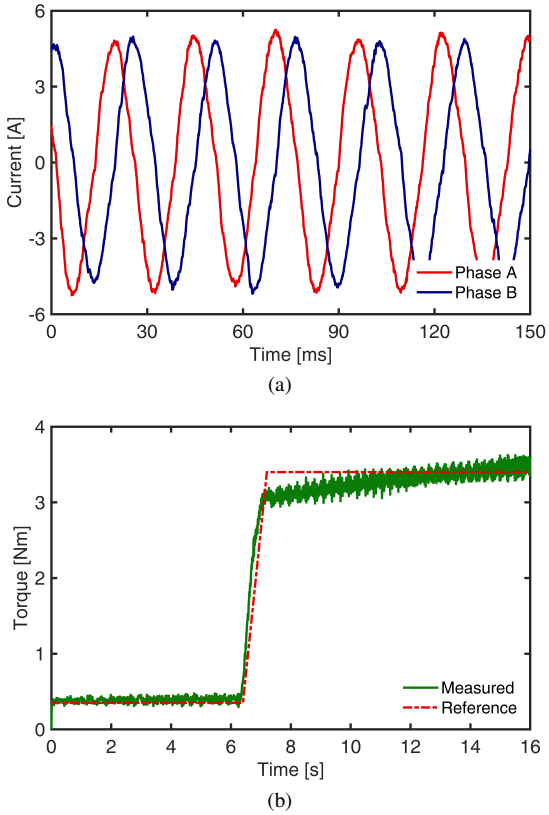

Fig. 5. The two-phase currents and the measured output torque with a change in the load torque are shown. Experimental results confirm remarkably low current ripple for this ultra-low phase inductance machine as a result of operating at a high switching frequency.

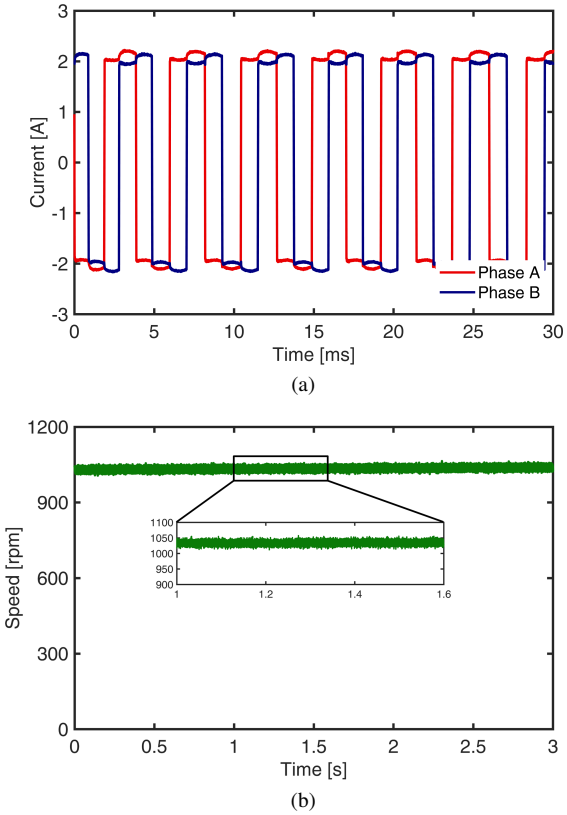

Fig. 6. The measured phase currents and shaft speed when the machine is operating under the square-wave control mode. The results show that the high rotor inertia efficiently filters the torque ripples induced by square-wave input currents, leading to a consistently stable rotor speed without any fluctuations.

machine is powered by the two single-phase SiC-based 10 kW inverter shown in Fig. 3b. Hardware-in-loop (HIL) simulations were performed using a dSPACE MicroLabBox to generate gate signals and conduct real-time phase current and output torque measurements, as well as encoder data interpretations.

The described field-oriented technique was implemented to control the machine under study, and its performance was evaluated through experimentation. The output voltages of the single-phase inverters applied to the PCB stator terminals are shown in Fig. 4. The figure also demonstrates how the machine is following the speed command. It should be noted that due to the high rotor inertia of this machine, the transient time to achieve the commanded speed is relatively long. The speed controller was meticulously designed, taking into account the mechanical system time constant, to ensure stability during these transient periods.

The machine's response to a sudden change in load torque is shown in Fig. 5, which illustrates the nearly sinusoidal phase current waveforms with negligible ripple, thanks to a high switching frequency of 65 kHz. It should be noted that in Fig. 4 and Fig. 5, the current and voltage plots cover a significantly shorter time period compared to the mechanical parameter waveforms, i.e., speed and torque, to offer a more detailed view of the current and voltage waveforms.

Coreless machines, in the presence of high-frequency current harmonics may still experience power losses in the rotor magnets and back-iron [10]. Experimental results have demonstrated that by employing a high switching frequency, the phase currents become nearly sinusoidal with low harmonic content. The thermal image included in Fig. 3c illustrates that at an ambient temperature of 27°C, the rotor PMs and back-iron experience minimal temperature rise when the machine operates at steady-state with sinusoidal currents (using FOC mode) with a high switching frequency. This finding indicates that the high-frequency losses in the PMs and back-iron during machine operation are negligible.

The square-wave control was also implemented, which is activated when speed commands exceed the rated speed or when an encoder malfunction occurs. The reference current generator block depicted in Fig. 1b produces square-wave phase current commands based on the rotor position and the desired speed. Subsequently, the input current is regulated by hysteresis current control blocks. With a high switching frequency, it becomes feasible to achieve smooth square-wave phase currents. The measured phase currents, when the machine was operating with square-wave control mode at a constant commanded speed, are shown in Fig. 6. The measured speed shows that despite the high torque ripple

caused by square-wave phase currents, the high-inertia of the rotor effectively filters it out, resulting in an smooth machine operation.

V. Conclusion

In this paper, a dual-mode control system was introduced for coreless AFPM machines, featuring ultra-low phase inductance and a high pole count. The performance of the drive system with the field-oriented control mode was experimentally investigated, and the results showed that a nearly sinusoidal phase current is achievable for the coreless machines employing a SiC-based inverter with a high switching frequency. Additionally, the square-wave control mode was implemented to expand the machine's speed range, capitalizing on the distinctive characteristics of coreless machines, such as the absence of core losses and negligible torque ripple. The square-wave control eliminated the need for high-precision encoders at ultra-high speeds, enabling the use of Hall effect sensors or sensorless drive schemes. Moreover, this control mode fully utilizes the DC-link voltage to further extend the machine operating range. Experimental results demonstrated that the high-frequency torque ripple, when the machine operates under this mode, effectively filters out due to the high inertia of the AFPM machine's rotor.

Acknowledgment

This paper is based upon work supported by the National Science Foundation (NSF) under Award No. #1809876. Any opinions, findings, and conclusions, or recommendations expressed in this material are those of the authors and do not necessarily reflect the views of the NSF. The support of Ansys Inc., Regal Rexnord Corp., and University of Kentucky the L. Stanley Pigman Chair in Power Endowment is also gratefully acknowledged.

References

[1] F. Marcolini, G. De Donato, F. G. Capponi, M. Incurvati, and F. Caricchi, "Novel multiphysics design methodology for coreless axial flux permanent magnet machines," *IEEE Transactions on Industry Applications*, pp. 1–11, 2023.

[2] F. Nishanth, J. Van Verdeghem, and E. L. Severson, "A review of axial flux permanent magnet machine technology," *IEEE Transactions on Industry Applications*, vol. 59, no. 4, pp. 3920–3933, 2023.

[3] V. Rallabandi, N. Taran, D. M. Ionel, and J. F. Eastham, "Coreless multidisc axial flux PM machine with carbon nanotube windings," *IEEE Transactions on Magnetics*, vol. 53, no. 6, pp. 1–4, 2017.

[4] N. Taran, V. Rallabandi, G. Heins, and D. M. Ionel, "Systematically exploring the effects of pole count on the performance and cost limits of ultrahigh efficiency fractional hp axial flux PM machines," *IEEE Transactions on Industry Applications*, vol. 56, no. 1, pp. 117–127, 2020.

[5] O. Taqavi and S. Mirimani, "Design aspects, winding arrangements and applications of printed circuit board motors: A comprehensive review," *IET Electric Power Applications*, vol. 14, pp. 1505–1518, 09 2020.

[6] A. Hembel and B. Sarlioglu, "PCB winding for electric machines with integrated 3d printed heat exchanger," in *2022 IEEE Transportation Electrification Conference Expo (ITEC)*, 2022, pp. 421–426.

[7] F. Marcolini, G. D. Donato, F. Giulii Capponi, M. Incurvati, and F. Caricchi, "On winding manufacturing technologies for coreless axial-flux permanent-magnet machines," in *2023 IEEE Workshop on Electrical Machines Design, Control and Diagnosis (WEMDCD)*, 2023, pp. 1–7.

[8] Y. Chulaee, D. Lewis, A. Mohammadi, G. Heins, D. Patterson, and D. M. Ionel, "Circulating and eddy current losses in coreless axial flux PM machine stators with PCB windings," *IEEE Transactions on Industry Applications*, pp. 1–11, 2023.

[9] A. K. Morya, M. C. Gardner, B. Anvari, L. Liu, A. G. Yepes, J. Doval-Gandoy, and H. A. Toliyat, "Wide bandgap devices in AC electric drives: Opportunities and challenges," *IEEE Trans. on Transportation Electrification*, vol. 5, no. 1, pp. 3–20, 2019.

[10] M. Leandro, N. Bianchi, M. Molinas, and R. B. Ummaneni, "Low inductance effects on electric drives using slotless permanent magnet motors: A framework for performance analysis," in *IEEE IEMDC 2019*, 2019, pp. 1099–1105.

[11] M. Rosu, P. Zhou, D. Lin, D. Ionel, M. Popescu, F. Blaabjerg, V. Rallabandi, and D. Staton, *"Multiphysics Simulation by Design for Electrical Machines, Power Electronics and Drives"*, J. Wiley - IEEE Press, 2017.

[12] M. S. Islam, R. Mikail, and I. Husain, "Field weakening operation of slotless permanent magnet machines using stator embedded inductor," *IEEE Transactions on Industry Applications*, vol. 57, no. 3, pp. 2387–2397, 2021.

[13] O. Ellabban and H. Abu-Rub, "An overview for the z-source converter in motor drive applications," *Renewable and Sustainable Energy Reviews*, vol. 61, pp. 537–555, 2016.

[14] D. Zhang, M. Zhou, C. Wang, and X. You, "A single-current-regulator flux-weakening control for PMSM under square-wave mode with wider operation range," *IEEE Transactions on Transportation Electrification*, vol. 8, no. 1, pp. 1063–1071, 2022.

[15] *Ansys Electronics Desktop, Maxwell, version 23.1, 2023, ANSYS Inc.*

[16] P. Han, D. Lawhorn, Y. Chulaee, D. Lewis, G. Heins, and D. M. Ionel, "Design optimization and experimental study of coreless axial-flux PM machines with wave winding PCB stators," in *2021 IEEE Energy Conversion Congress and Exposition (ECCE)*, 2021, pp. 4347–4352.

[17] D. Lawhorn, P. Han, D. Lewis, Y. Chulaee, and D. M. Ionel, "On the design of coreless permanent magnet machines for electric aircraft propulsion," in *2021 IEEE Transportation Electrification Conference Expo (ITEC)*, 2021, pp. 278–283.

[18] Y. Chulaee, D. Lewis, M. Vatani, J. F. Eashtam, and D. M. Ionel, "Torque and power capabilities of coreless axial flux machines with surface PMs and halbach array rotors," in *2023 IEEE International Electric Machines and Drives Conference (IEMDC)*, 2023, pp. 1–6.

[19] N. Mohan, *"Electric Machines and Drives"*, J. Wiley, 2017.

[20] B.-K. Lee and M. Ehsani, "Advanced simulation model for brushless DC motor drives," *Electric Power Components and Systems*, vol. 31, no. 9, pp. 841–868, 2003.

[21] Y. Chulaee, H. A. Zarchi, and S. I. H. Sabzevari, "State estimation for sensorless control of BLDC machine with particle filter algorithm," in *2019 10th International Power Electronics, Drive Systems and Technologies Conference (PEDSTC)*, 2019, pp. 172–177.

[22] J. Chen, X. Yuan, F. Blaabjerg, and C. H. T. Lee, "Overview of fundamental frequency sensorless algorithms for ac motors: A unified perspective," *IEEE Journal of Emerging and Selected Topics in Power Electronics*, vol. 11, no. 1, pp. 915–931, 2023.